A numerical investigation into the influence of the interfacial transition zone on the permeability of partially saturated cement paste between aggregate surfaces

Li, Kai; Stroeven, Piet; Stroeven, Martijn; Sluys, Lambertus J.

DOI
10.1016/j.cemconres.2017.09.005

Publication date
2017

Document Version
Final published version

Published in
Cement and Concrete Research

Cement and Concrete Research 102 (2017) 99–108

Contents lists available at ScienceDirect

Cement and Concrete Research

journal homepage: www.elsevier.com/locate/cemconres

A numerical investigation into the influence of the interfacial transition zone on the permeability of partially saturated cement paste between aggregate surfaces

Kai Li*, Piet Stroeven, Martijn Stroeven, Lambertus J. Sluys

Faculty of Civil Engineering and Geosciences, Delft University of Technology, Stevinweg 1, 2628 CN Delft, The Netherlands

ARTICLE INFO

Keywords:
Concrete (E)
Permeability (C)
Water saturation degree
Interfacial transition zone (B)
Modelling (E)

ABSTRACT

The interfacial transition zones (ITZs) are supposed to promote fluid transport through concrete. As a consequence, one would expect an increase in permeability with an increasing aggregate fraction. This has been shown in some experiments, however, the opposite effect is observed as well. The permeability ratio of ITZ to matrix seems to be a key parameter in interpreting this controversial phenomenon. A higher ratio favors the flow of water through the interface zone. This work aims at studying this ratio at various conditions (*i.e.*, hydration degree, water/cement ratio, particle size range and water saturation degree) using a numerical model, so that the influence of the ITZ on the permeability of cementitious composites can be better understood. The findings presented in this paper can provide a new perspective on controversial experimental results as to the effect of the ITZ on transport capacity.

1. Introduction

Concrete on meso-level is generally considered a three-phase material. Major components are the cement matrix and aggregate particles. However, modifications of the cement structure around aggregate surfaces referred to by the interface zone can be viewed as the third phase. This ITZ reveals significant compositional differences as compared to the bulk paste. These differences are most significant very close to the aggregate surface and gradually diminish away from the aggregate grain surface to become insignificant at a certain distance (15–50 μm) [1]. The ITZ differs from bulk paste in porosity, pore size and also in the complementary anhydrous cement and C-S-H (calcium silicate hydrate) contents. In general, the ITZ contains less anhydrous cement grains, larger pores and higher porosity, resulting in higher transport properties (*i.e.*, permeability, diffusivity and conductivity) in contrast to that of bulk paste. The ITZ fraction goes up and the spacing between adjacent ITZs decreases at increased aggregate content, both leading to a larger degree of ITZ overlap. According to the ITZ percolation theory [2], the ITZs will mutually connect and thus fast-conduction pathways will be formed through the material once the aggregate content reaches a threshold value. In theory, the permeability of concrete should rise at the increased aggregate content and a sudden increase can be expected at the percolation threshold [3]. This is confirmed by Halamickova's work [4]. Yet, it is not always the case in practice. Contradictory results are also experimentally obtained in permeability tests. As an example, the permeability of concrete is observed to go down at an increased aggregate fraction in [5]. A similar controversy exists regarding the influence of the ITZ on chloride diffusivity and electrical conductivity [6–8].

Although earlier studies [8–10] have been performed to better understand why such contradictory observations exist, the ITZ structures were in general simply treated as homogenous layers covering the surface of hydrating cement grains. Furthermore, the existing models [11–12] that have looked at the effect of technological parameters on the contrast ratio of ITZ to bulk cement paste are mostly based on diffusion rather than on permeation. The objective of this paper is to study the influence of several technological parameters (*i.e.*, hydration degree, water/cement ratio, cement particle size range and water saturation degree) on the permeability of the ITZ and bulk paste. For that purpose, the ITZ is numerically constructed using a DEM-based (Discrete Element Modelling) approach, as will be described in Section 2.1. It is expected that the presented work can provide a new perspective on this controversial experimental phenomenon.

In general, there exists a set of competing effects when adding aggregates to the cement matrix [5,9]. On the one hand, porous matrix is replaced by impermeable aggregate, resulting in a decline in the total porosity and thus permeability. This is denoted as the dilution effect. The enlarged amount of aggregates also leads to an increase in the

* Corresponding author.
E-mail address: K.Li-1@tudelft.nl (K. Li).

http://dx.doi.org/10.1016/j.cemconres.2017.09.005
Received 21 July 2017; Received in revised form 25 August 2017; Accepted 5 September 2017
Available online 19 September 2017
0008-8846/

tortuosity of transport paths [13]. These two effects mainly result in reduced transport properties. This is counteracted by the enlarged area of the more porous ITZ, facilitating the ingress of fluid and thus promotes the transport properties. As a consequence, the effects of aggregates on concrete's transport properties depend on which factor will dominate the scene. According to Garboczi and Bentz [14], the conductivity ratio of ITZ to matrix paste ($\sigma_{ITZ}/\sigma_{matrix}$) is an important parameter in determining the relationship between mortar conductivity and the sand volume fraction. It is found that a value of the $\sigma_{ITZ}/\sigma_{matrix}$ of at least 10 to 20 is required to compensate for detrimental effects so that the conductivity of mortar can be enhanced at increased sand content. Later, Shane et al. [15] further pointed out that $\sigma_{ITZ}/\sigma_{matrix}$ varies with the hydration time and is actually a function of the degree of hydration. The peak with a value of approximately 7 only occurs when the degree of hydration is around 0.7. This value is below 10, so it is not likely that the ITZ will significantly enhance the conductivity of mortar [15]. From permeability studies it is already known that permeability is much more sensitive to pore size than conductivity is [4–5]. Due to the large pores in the ITZ region, the permeability ratio between ITZ and matrix paste ($\kappa_{ITZ}/\kappa_{matrix}$) is expected to be much larger than the conductivity ratio $\sigma_{ITZ}/\sigma_{matrix}$. In reality, the difference may be even larger because of microcracks in concrete. Nevertheless, the threshold value for $\sigma_{ITZ}/\sigma_{matrix}$ and $\kappa_{ITZ}/\kappa_{matrix}$ that is used to evaluate the influence of the ITZ on transport properties of cementitious material is supposed to be similar. When $\kappa_{ITZ}/\kappa_{matrix}$ is exceeding the threshold value, the ITZ effect will outweigh the other effects of the aggregate, so that the ITZ is supposed to enhance the permeability of concrete. Otherwise, the dilution and tortuosity effects become dominant, which leads to a reduced permeability at an increased aggregate content. Fig. 1 shows the different effects of the ITZ on the conductivity of mortar at increasing sand volume fraction. It seems that the conductivity ratio between the ITZ and the bulk matrix should exceed a threshold so that the ITZ would promote the conductivity of mortar. However, relatively little is known about the quantitative differences between the permeability of the ITZ and the bulk paste. Additionally, cementitious materials in service are seldom fully saturated due to water evaporation. Yet, the saturation degree of specimens has been proven an important factor governing permeability [16–19]. It should likewise affect the value of $\kappa_{ITZ}/\kappa_{matrix}$. Unfortunately, experimental research on the $\kappa_{ITZ}/\kappa_{matrix}$ relationship to the permeability of concrete has not been conducted yet. It will constitute therefore the main content of the presented work. Since experimental measurements on permeability of cementitious materials usually require specialized equipment and long periods of time to complete, a modelling approach is employed in the present case due to its economic and reliable characteristics. Drying-induced micro-cracking is another crucial factor affecting the transport properties of concrete and thus the permeability ratio ($\kappa_{ITZ}/\kappa_{matrix}$), as shown by recent experimental and 3D modelling studies [20–23]. Due to the nature of ITZ, cracks in practice tend to initiate in this zone. Once these cracks coalesce, the water ingress process could be promoted, resulting in a higher $\kappa_{ITZ}/\kappa_{matrix}$. Moreover, air voids may exist in mortars or concretes in real experiments due to inadequate compaction and thus exaggerate the ITZ effect. This may be the reason why the measured permeability in [4] goes up with the increasing aggregate content. However, the influence of micro-cracks on water transport of cementitious materials is not within the scope of this study.

In this paper, a systematic study is performed to evaluate the influence of several parameters (*i.e.*, degree of hydration, water/cement ratio, particle size range and saturation degree) on the value of $\kappa_{ITZ}/\kappa_{matrix}$. A brief introduction on the developed numerical approach will be given in Section 2. Since the full methodology has been presented in detail earlier, the interested readers are referred to the relevant publications for more information [18,24]. The respective effects of degree of hydration, water/cement ratio, particle size range and saturation degree on the permeability ratio of ITZ to matrix paste will be presented in Section 3. The value of $\kappa_{ITZ}/\kappa_{matrix}$ is found to strongly depend on the sample's conditions (degree of hydration, water/cement ratio, particle size range and saturation degree). The findings presented in this work are compared with the results from [15].

2. Numerical approach

Since the developed modelling technique has been presented in full detail in [18,24], only a brief introduction is given here. Nevertheless, enough information will be provided in this section to enable the readers to understand how the modelling operation is performed.

2.1. Generation of the bulk material and ITZ

It is well known that the origin of the ITZ derives from the cement particles packing against the aggregate surface [1]. Since the aggregate size is in general much larger than that of the cement grains, the aggregate surface can actually be considered flat. When the cement

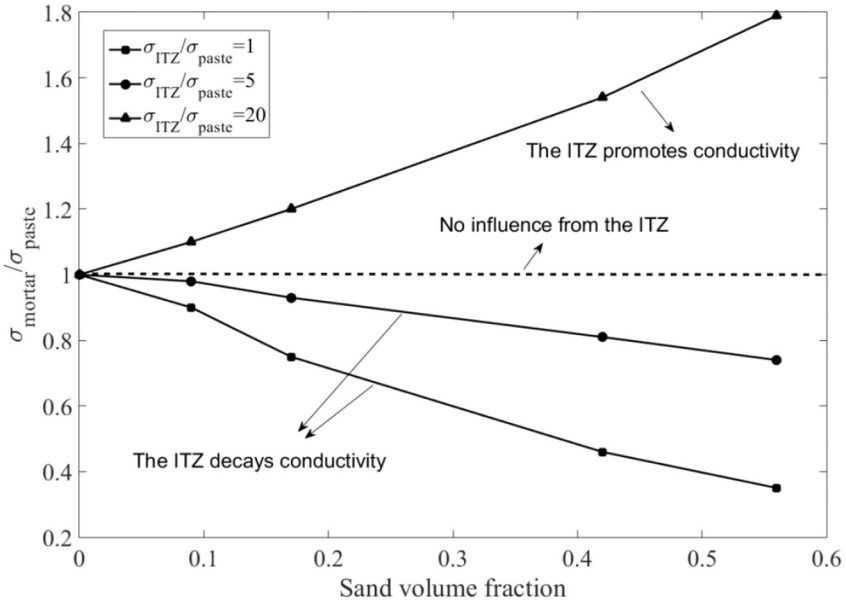

Fig. 1. Conductivity ratio between mortar and cement paste (σ_m/σ_p) is shown as a function of sand concentration for several values of the interfacial zone conductivity to bulk matrix ($\sigma_{ITZ}/\sigma_{matrix}$). Dashed line indicates no difference in conductivity between mortar and cement paste at a certain threshold of $\sigma_{ITZ}/\sigma_{matrix}$. The data shown in this figure are obtained from [8].

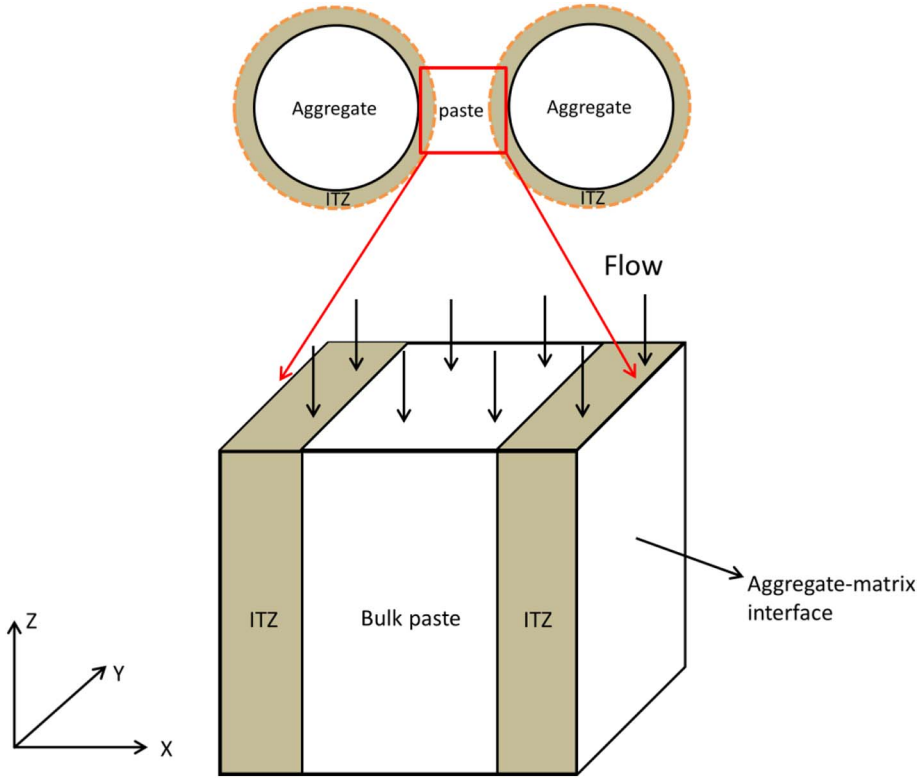

Fig. 2. Schematic illustration of the ITZ structure in our modelling techniques.

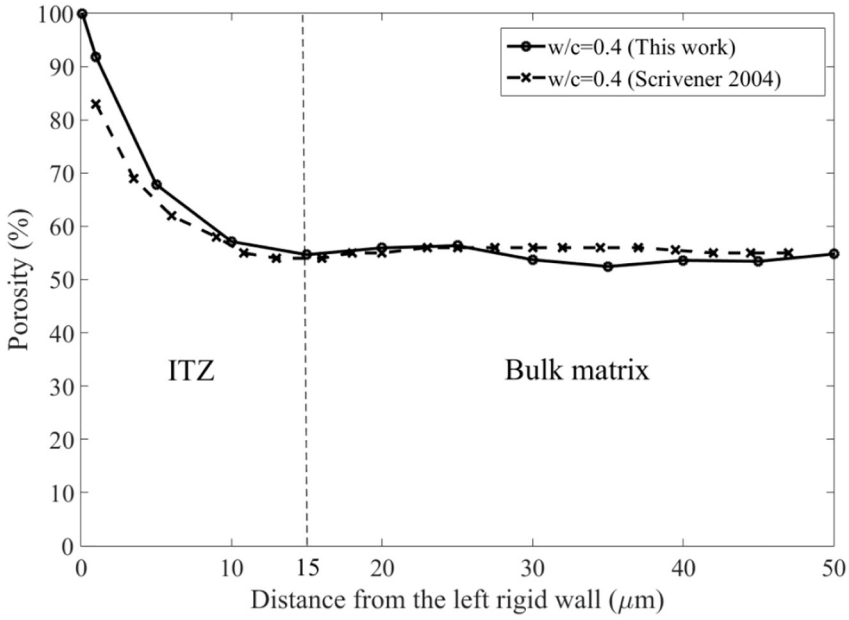

Fig. 3. Porosity gradient existing in the ITZ of fresh specimen. Solid line represents the simulation results from this study, while the dashed line is obtained from experimental data [1].

particles approach this surface of the aggregate, the packing constraints lead in a global sense to a gradient structure [25]. The differences in structure gradually diminish away from the aggregate surface to eventually become insignificant at a certain distance from the aggregate surface, as illustrated in Fig. 2.

To numerically construct the ITZ structure, the following assumptions are made in this work. (1) Since the size of aggregate is much larger than that of cement grain, the aggregate's surface is assumed to be planar while cement particles are still treated as spheres; (2) Aggregate size, shape and volume fraction do not affect the ITZ characteristics; (3) Aggregates are separated far enough so that they do not interfere with each other. So, to start with, two parallel planes were fixed in the X-direction to represent the surfaces of neighbouring aggregate grains. Limitations in Y- and *Z*-direction of specimens were achieved by periodic boundaries. Fresh cement grains were modelled as spheres for simplification purposes. All particles were initially generated in a larger cuboidal container with two rigid walls in X-direction and four periodic ones in the other Cartesian coordinate directions. During the dynamic packing process, the size of the container was gradually diminished until the container reached its desired size and the structure its objected packing density. Various interactions (particle-particle, particle-rigid wall) were taken into account to simulate the mixing process. Herein, the ultimate specimen size was set as 100 μm, commonly considered as a representative size of virtual

cementitious material in the used size range. The number of particles depends on the pre-set water/cement ratio (that is, packing density) and particle size distribution. In the present case, the water/cement ratio was set to 0.4 and the Rosin Rammler function was chosen to represent the particle size distribution, ranging from 1 to 30 μm (the number of particles were of the order of 2×10^4 in a 100 μm computational cube). Note that the water/cement ratio and the particle size range will be varied later to investigate the effects of the changes in these two parameters on the $\kappa_{ITZ}/\kappa_{matrix}$ function, as will be described in Sections 3.2 and 3.3.

A serial sectioning operation was conducted along the X axis to measure the porosity as a function of the distance to the aggregate surface. Due to symmetry reasons, only the results of the 50 μm thick region neighbouring the left rigid wall are plotted and compared to the data obtained by experimental measurements [1], as given in Fig. 3. The gradient porosity curve obtained in this way is found to be in satisfactory agreement with experimental data, validating the modelled ITZ and bulk paste structure. This leaves the inner boundary of the ITZ to be assessed in an objective way, so that the respective contributions to the permeability of concrete by ITZ and bulk matrix can be determined. In this work, the border of the ITZ is associated with the point where the porosity will start exceeding the bulk value by a threshold of 2%. A thickness of 15 μm was found as the ITZ thickness in this case, leaving a region of 70 ($= 100–2 \times 15$) μm of bulk zone. Note that no clear border exists in practice between the ITZ and the matrix due to pores in the ITZ connecting with pores in the bulk zone [26]. This complex phenomenon is not within the scope of the presented numerical study. Although the hydration time, water/cement ratio and particle size range have been proven to affect the ITZ thickness, a constant value of 15 μm has been consistently used in this work to keep it in accordance with the setup in [15].

2.2. Three-dimensional matured microstructures

In the next stage, the densified structure retrieved from the particle packing modelling is used as input for the hydration simulation discussed in this section. Similar to a real experimental setup, the fresh specimen needs to react with water to produce matured samples. The vector-based XIPKM (Extended Integrated Particle Kinetics Model) was used to simulate the hydration process [27]. The major cement compounds, *i.e.*, tricalcium silicate (C_3S), dicalcium silicate (C_2S), tricalcium aluminate (C_3A) and tetracalcium aluminoferrite (C_4AF), are taken into account. The volume fraction of these four phases of the cement clinker were 61%, 20%, 8% and 11%, respectively. The interested readers are referred to [27] for more details on XIPKM. The DEM packed particulate microstructure serves as an input for XIPKM. The main hydration product, calcium silicate hydrate (C-S-H), is treated as a homogenous and impermeable material surrounding the hydrating cement grains. Although C-S-H has been proven to be a porous medium, its structure and formation mechanism are still not clear [28–29]. So, no more details on the internal structure of C-S-H are taken into account. Due to the hydration reactions, cement particles grow concentrically to fill the free space, resulting in a spatial pore network structure with complex geometric and topological properties. The simulation stops when all available water has been consumed. It is assumed that the ingress of water during the permeability test does not cause further hydration and does not affect the degree of hydration. Microstructures at various hydration ages were chosen for further study.

2.3. Pore delineation and measuring in hardened microstructures

To measure the permeability from a so obtained hydrated structure, the Double Random Multiple Tree Structuring (DRaMuTS) method was used to assess the topology of the pore structure of the abovementioned virtual matured material. DRaMuTS is a robotics-inspired technique, and has been shown able to perform the porosimetry operation and provide reliable results in [30]. It starts by distributing random points throughout the virtual structure of which only the points situated in pore space are used for further analysis. 10^5 points have been shown able to provide precise data at reasonable computational efforts in [18]. The points or nodes dispersed inside the pores are – if possible – connected by unobstructed straight line segments. The result is a tree-like structure inside the capillary pore network structure of the specimen, making it possible characterizing its topological properties. Hence, isolated pores and dead-end pores branching off the continuous main channels can be distinguished and taken out from the flow simulation operation at a later stage to optimize performance.

In the next step, local pore volume needs to be assessed to determine the local pore size. A star volume measuring (SVM) approach is applied for that purpose. Each point of a second random system is the nucleus of a star of which a large number of its random rays is used to estimate the size of the representative sphere. More relevant details can be found in [31]. The pore information obtained in this way, along with the pore connectivity will be used as input parameters for permeability calculations in the next section.

2.4. Permeability calculation of microstructures at various water saturation degrees

A tube network model was employed in this work to simulate the fluid flow through the pore network system of the virtual hydrated specimens. Compared to another popular modelling approach, *i.e.*, the Lattice Boltzmann method [16], the tube model can be directly applied to the virtual materials. It does not require the structure to be discretized into small voxels. The discretization process required by the Lattice Boltzmann method inevitably results in the resolution issue and the accuracy of this approach therefore strongly depends on the resolution limit. The lower minimum resolution leads to more accurate result, but also requires more computational effort especially when there is a large difference between the smallest and largest pores in the system. In the tube model, a structure consisting of cylindrical tubes was constructed to represent the pore channels using the locations and sizes of the pores (pore information is from porosimetry operation as described in Section 2.3). The influence of actual pore shape on permeability estimation is also accounted for, as described in detail in [18]. Only the main channels or trunks are considered and extracted from the system for permeability calculations, while the isolated and dead-end pores are neglected in this study. The main trunk is defined as the direct path through pore space from the bottom to the top of the specimen. The water flow through the specimen is activated by an applied pressure gradient between inlet and outlet nodes located at the top and bottom surfaces. Similar to a real permeability test, Darcy's law is also used in the numerical simulation to calculate permeability. However, applying Darcy's equation requires the specimen to be fully saturated. Consequently, the pore space is always assumed to be saturated with water in simulations. Later we show how to simulate partially saturated cement paste without violating the condition imposed on using Darcy's law. The ITZ and bulk paste were simply treated as independent phases. This treatment is strictly speaking not true since some pores in the ITZ and cement matrix actually interconnect. This effect is not taken into account in this work.

As stated earlier, full saturation is assumed for the specimens. Unfortunately, this is not always the case in practice. Although the specimens in experiments are immersed into water for long periods of time to ensure their fully saturated states, it is quite difficult (if not impossible) to reach and maintain this state [32]. In fact, water evaporation inevitably occurs due to humidity changes inside the materials and this results in samples with variable water content [33]. The major influence of the water saturation degree on permeability of cement paste has been studied in [16–18]. It is found that water permeability significantly decreases with a reduced degree of water saturation. In

reality, the degree of saturation should increase when the sample is exposed to water during the permeability test. However, this was not taken into account in the model. In fact, the empty pores (filled by air) block the paths for water transport with an identical result as solid grains would have. A blocking algorithm is therefore developed by the present authors to generate the samples at various water saturation degrees, as described in detail in [18]. Impermeable solid spheres are put at the positions where water is assumed to have evaporated to block the transport paths. This occurs sequentially starting from the largest pores in accordance with the Kelvin-Laplace law that tells that air will occupy the largest pores first. This procedure can be easily carried out since all pores are already sorted by size and stored in the above-mentioned porosimetry operation. In this way, the samples at different saturation degrees can be well represented. The permeability of such partially saturated specimens calculated from the tube model show a satisfactory agreement with other published data, validating our numerical approach [18]. The blocking algorithm is used in this work to obtain the specimens at various saturation degrees. Since large pores predominantly exists in the ITZ, it can be expected that water evaporation in the ITZ differs from that in the bulk phase. This inevitably affects the permeability of the ITZ and cement matrix and thus the permeability ratio. The influence of water saturation degree on the $\kappa_{ITZ}/\kappa_{matrix}$ function will be described in Section 3.4.

3. Results

The methodology described in Section 2 has been applied to calculate the permeability ratio of the ITZ and the bulk cement matrix ($\kappa_{ITZ}/\kappa_{matrix}$) at various conditions (*i.e.*, degree of hydration, water/cement ratio, particle size range and water saturation degree), while the reference case is a fully saturated specimen with water/cement ratio 0.4 and particle size range of [1 μm, 30 μm]. The results are presented in this section. Partially saturated specimens will be considered in Section 3.4 while the samples in other cases are always in the fully saturated state.

3.1. Influence of the degree of hydration

The permeability of ITZ and matrix paste at different degrees of hydration are respectively plotted in Fig. 4. Degree of hydration (DOH) is defined as the amount of reacted cement at a certain hydration time divided by the total amount of cement at the initial stage. As a first observation, the permeability of ITZ and bulk region show a downward trend as hydration proceeds. This is attributed to the fact that the structure gradually densifies at prolonged hydration periods. Moreover, the two curves in Fig. 4 show a similar (almost log-linear) pattern until

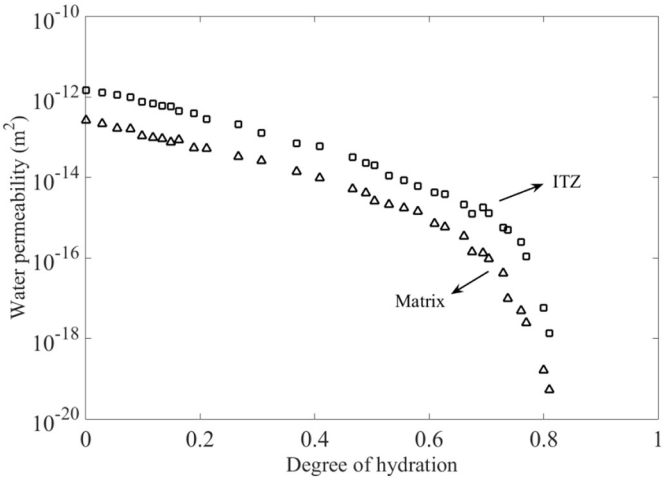

Fig. 4. Permeability of the ITZ and cement matrix at various hydration degrees.

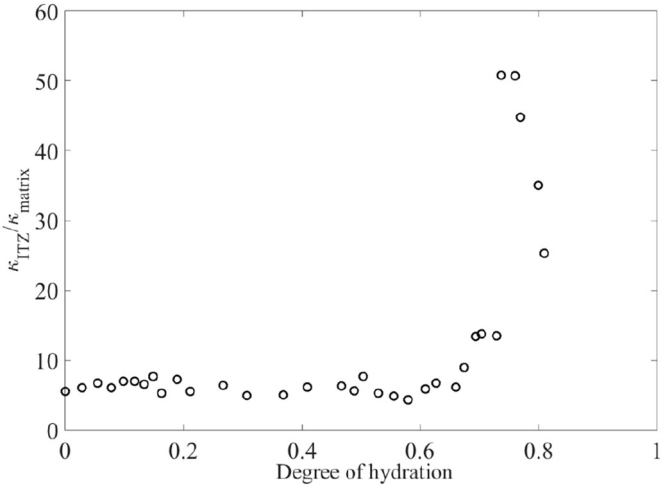

Fig. 5. The permeability ratio of the ITZ and cement matrix ($\kappa_{ITZ}/\kappa_{matrix}$) at various hydration degrees.

a sharp drop in permeability is found to occur earlier in the bulk matrix than in the ITZ.

In general, they both slightly decrease at first and then sharply go down after a certain point, which agrees well with the findings as reported in [34]. The reason why such distinct trend is observed can be explained as follows. At the early stages of hydration, the pore system is highly connected. In such a highly connected pore system, pore size predominantly governs the permeability. The gradual decline in pore size results therefore in a similar smooth decline in permeability. Once the pore system starts to de-percolate, pore connectivity becomes the dominant parameter. As a result, a distinct reduction in pore connectivity during prolonged hydration leads to the sharp drop in permeability. The ITZ contains larger pores and higher porosity, resulting in a higher permeability level at equal DOH than bulk cement paste. When the system reaches its ultimate degree of hydration, the difference (in terms of porosity) between the ITZ and bulk phase still exists, resulting in different permeability values.

In Fig. 5, $\kappa_{ITZ}/\kappa_{matrix}$ is plotted as a function of DOH. Since the permeability in ITZ and bulk paste are almost proportionally declining with hydration degree early in the hydration process, the ratio of both remains almost constant, with a value of about 5. At a higher DOH, the pore de-percolation starts leading to a sharp decline in permeability in both cases. Yet, the pore de-percolation effect can be expected to start earlier in bulk because of the finer pore network structure. The difference in the pore de-percolation processes of bulk and ITZ will therefore reveal a distinct peak (of about 52) in $\kappa_{ITZ}/\kappa_{matrix}$ at a DOH of about 0.76. After this peak value, this ratio will decline at prolonged DOH until hydration ends at the ultimate degree of hydration due to the sharp drop in the permeability of both ITZ and bulk. According to Shane [15], the permeability ratio of the ITZ and the cement matrix should be in the order of 10–20 to overcome the dilution effect of the aggregate particles, so that the ITZ would promote the transport-based properties. In this study, except for a narrow region (DOH between 0.7 and 0.8), the $\kappa_{ITZ}/\kappa_{matrix}$ is in general below 10. This indicates that it is not likely that the addition of aggregates to cement paste will enhance the permeability of concrete.

To the authors' knowledge, there does not exist direct available data about $\kappa_{ITZ}/\kappa_{matrix}$ *versus* DOH in the literature. As an alternative, the numerical data (already verified by experimental results) about the conductivity ratio of ITZ to matrix paste ($\sigma_{ITZ}/\sigma_{matrix}$) from [15] was used to qualitatively validate the observed relationship in Fig. 5. Permeability and conductivity both belong to transport-based properties, so the general features of the $\kappa_{ITZ}/\kappa_{matrix}$ and $\sigma_{ITZ}/\sigma_{matrix}$ graphs should be similar, making the comparison in the present case acceptable. The outcome is presented in Fig. 6. The two curves in Fig. 6 show a similar

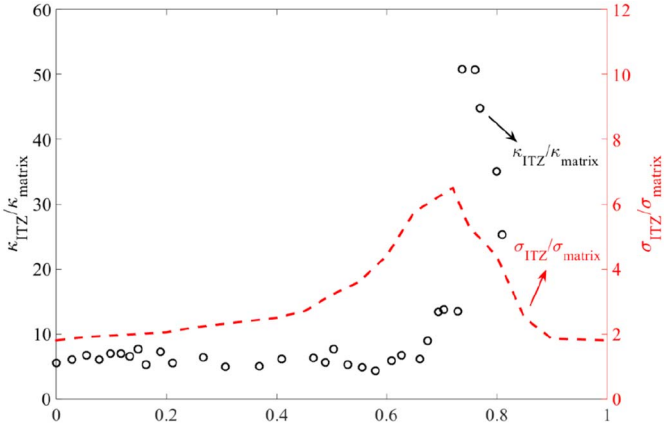

Fig. 6. The $\kappa_{ITZ}/\kappa_{matrix}$ at various hydration degrees obtained in this study and the conductivity ratio curve according to [15].

tendency and a peak is observed at approximately similar DOH in both cases. However, the maximum value of $\kappa_{ITZ}/\kappa_{matrix}$ (about 52) is much larger than that of $\sigma_{ITZ}/\sigma_{matrix}$ (around 7). A distinct difference like that can be explained by the Katz-Thompson equation [35–36],

$$\frac{\kappa_{ITZ}}{\kappa_{matrix}} = \frac{\sigma_{ITZ}}{\sigma_{matrix}} \frac{d_{c,ITZ}^2}{d_{c,matrix}^2} \tag{1}$$

where $d_{c,ITZ}$ and $d_{c,matrix}$ represent the critical pore diameter of ITZ and cement matrix, respectively. As the ITZ contains larger pores than the paste, $d_{c,ITZ}$ should be larger than $d_{c,matrix}$. This causes the permeability ratio in general to exceed the conductivity ratio. Also, the peak value of 52 observed in this study is well within the range (10 − 100) estimated in [15], and quite close to the calculated value of 35 in [8].

3.2. Influence of water/cement ratio

The influence of water/cement ratio (w/c) on the $\kappa_{ITZ}/\kappa_{matrix}$ *versus* DOH graph will be discussed in this section. The results are presented in Figs. 7–8. Note that water/cement ratio is the only parameter in this part of the study that is varied. The other parameters are kept constant. In general, a similar relationship between permeability and DOH is found in all cases while the sample with higher w/c has larger permeability. An increase in w/c also results in a later de-percolation phenomenon. This is the reason why the peak value of $\kappa_{ITZ}/\kappa_{matrix}$ shifts to the right with increasing values of w/c, as revealed by Fig. 8. The peak values of $\kappa_{ITZ}/\kappa_{matrix}$ in all samples are larger than 20, indicating that adding aggregates to cement paste may lead to an increased permeability of concrete. For the specimens that have a smaller $\kappa_{ITZ}/\kappa_{matrix}$, adding aggregates to cement may have a negative effect on the permeability of concrete due to dilution and tortuosity effects. Additionally, Fig. 7 shows that the hydration stops at a DOH equal to 0.63, 0.81 and 0.89 in the specimens with w/c of 0.3, 0.4 and 0.5, respectively. This is attributed to the different amounts of water available for cement hydration in the abovementioned structures, whereby a larger water content results in a larger value of the DOH. Fig. 7a shows that the hydration process of a specimen with $w/c = 0.3$ stops at DOH = 0.63 (before the de-percolation) since no water is available for further hydration. This is why the permeability of the specimen with $w/c = 0.3$ ends at a higher value than that of the sample with $w/c = 0.4$ and different permeability values for the ITZ and matrix are still observed at ultimate DOH. In the case of $w/c = 0.4$, for the ITZ and cement matrix a similar permeability is found because the difference in pore structure (*i.e.*, porosity and pore size) between the ITZ and matrix is diminished at ultimate DOH (after the de-percolation). Although the specimen with $w/c = 0.5$ reaches the highest DOH, the structure still does not de-percolate due to its greatest inherent porosity. As a consequence, no significant reduction in permeability is observed in the cases of $w/c = 0.5$.

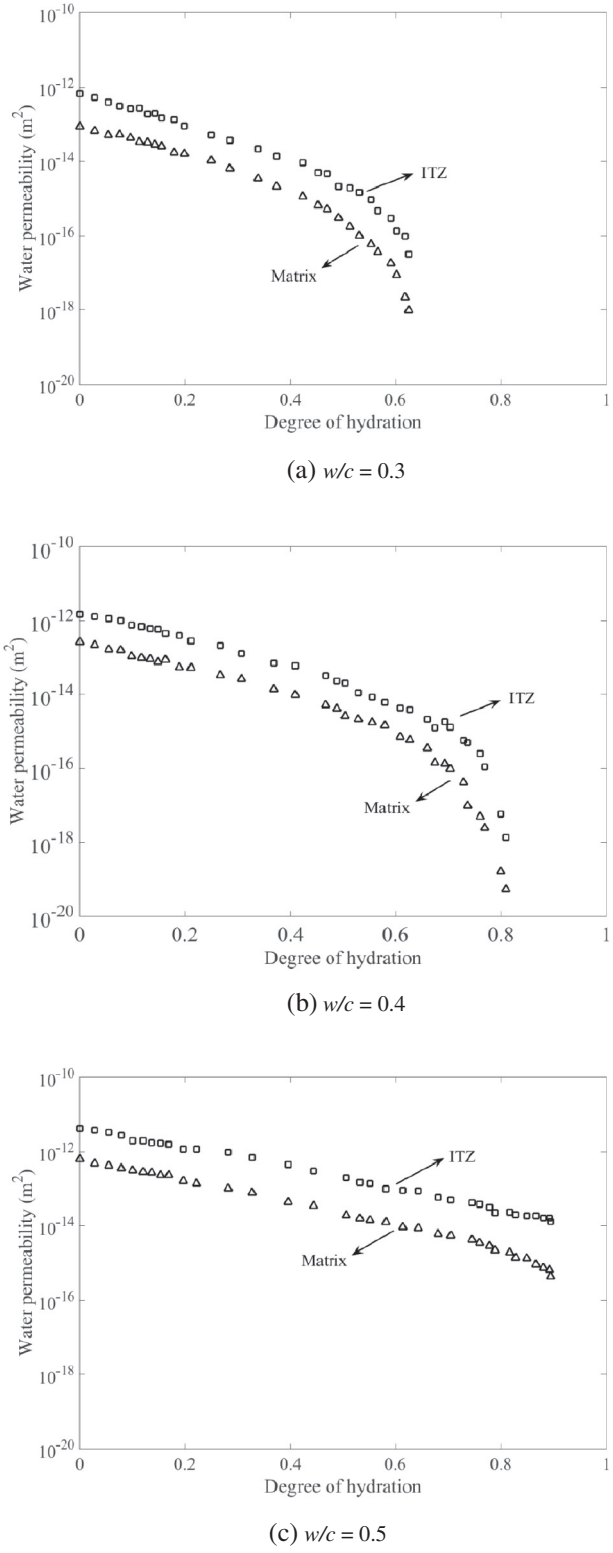

Fig. 7. Permeability of ITZ and matrix *versus* degree of hydration at different w/c.

3.3. Influence of particle size range

Since the particle size range has a significant influence on the hydration process and thus the permeability, its effects on the $\kappa_{ITZ}/\kappa_{matrix}$ curve are also investigated and presented in this section. Similar to

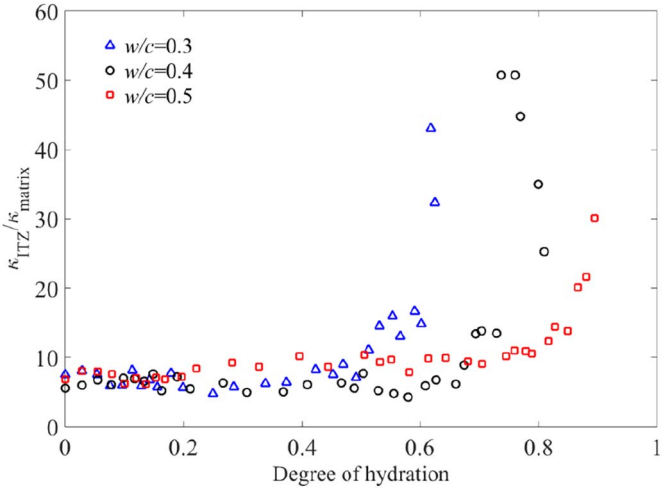

Fig. 8. $\kappa_{ITZ}/\kappa_{matrix}$ *versus* degree of hydration at different *w/c*.

Section 3.2, the relationship between the permeability of the ITZ and bulk paste with respect to the hydration degree at different particle size ranges (PSRs) is first shown in Fig. 9. The minimum particle size for all specimens was set to 1 μm. The maximum particle size for the PSR15, PSR30 and PSR45 specimens was set to 15 μm, 30 μm and 45 μm, respectively. The *w/c* was kept constant at 0.4 in this case. The general tendency observed in Fig. 9 is in accordance with the findings presented in the previous sections. Special attention needs to be given to the samples with PSR15 and PSR45 since they end at a higher permeability and the curves in Fig. 9a and c do not overlap at high degree of hydration in contrast to the PSR30 sample. This is attributed to the different compositions in these cases. PSR15 contains a large amount of small particles and PSR45 a small amount of large particles, while PSR30 is an intermediate case. The difference in composition results in a different hydration process and thus a different pore structure. As a consequence, although the hydration process of PSR15 and PSR30 samples stops at similar ultimate DOH, the structure of PSR15 specimen does not de-percolate similarly as that of PSR30. Hence, PSR15 achieves a higher permeability compared to PSR30. Moreover, the curves for PSR15 (Fig. 9a) do not overlap at high DOH, resulting in no apparent drop of the $\kappa_{ITZ}/\kappa_{matrix}$ for PSR15 in Fig. 10. In the case of PSR45, although there still exists a small amount of water for continuous hydration, the hydration process after DOH = 0.73 becomes very slow and the changes in structure are less significant for further consideration. So, the hydration process of PSR45 is assumed to stop at DOH = 0.73 (before the de-percolation point). Therefore, a dramatic decrease in permeability values of PSR45 samples do not occur. As a result, similar to PSR15, PSR45 also reaches a higher permeability compared to PSR30 and the curves for PSR45 (Fig. 9c) do not overlap at high DOH. Finally, the $\kappa_{ITZ}/\kappa_{matrix}$ level of the PSR45 sample seems to be higher than that of the other two cases. A possible reason may be that the assumption of a constant ITZ thickness in this work is not true. The influence of the particle size range on the ITZ structure has been shown in [37]. However, this effect is not taken into account in the presented study to maintain consistency with Shane's work [15].

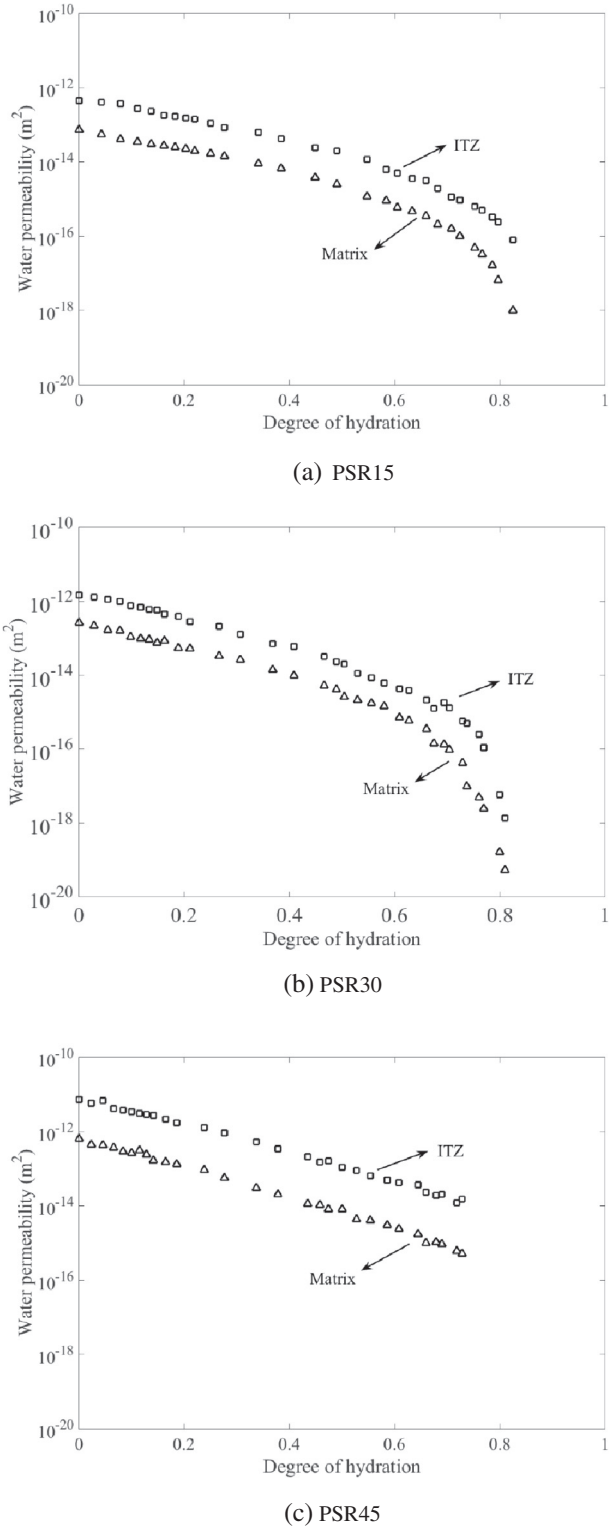

Fig. 9. Permeability of ITZ and matrix *versus* degree of hydration at different PSR. PSR15, PSR30 and PSR45 represents particle size range [1 μm, 15 μm], [1 μm, 30 μm] and [1 μm, 45 μm], respectively.

3.4. Influence of water saturation degree

Until now, all the samples used in this study were presumed at fully saturated state. However, this is not always the case in practice. Due to the humidity changes in the environment, water evaporation inevitably occurs inside samples. The significant effects of the water saturation degree (*S*) on permeability have been demonstrated in [16–18]. To simulate the water evaporation in the numerical model, the blocking algorithm as described in Section 2.4 was used to obtain samples at various saturation degrees. The data concerning the influence of water saturation degree on $\kappa_{ITZ}/\kappa_{matrix}$ are presented in Figs. 11–12. Large pores are easier to loose water in contrast to the small ones according to the Kelvin-Laplace equation. During the blocking operation for generating the partially saturated specimens, the large pores are first blocked at a decreasing degree of water saturation. Large pores

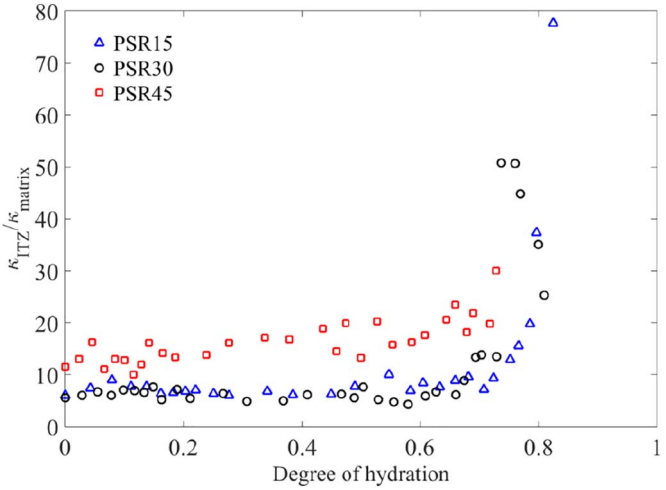

Fig. 10. $\kappa_{ITZ}/\kappa_{matrix}$ *versus* degree of hydration at different PSR.

predominantly exist in the ITZ region. This leads to a disproportional amount of blocked pores in the ITZ with respect to the bulk matrix for a given saturation degree. The difference between the ITZ and paste (in terms of pore structure) thus gradually decreases and finally disappears. Fig. 11 shows the permeability of the ITZ gradually to approach that of the cement matrix when S is reduced from 100% to 67%, and the two curves seem to overlap at $S = 44\%$. This indicates that the difference in permeability between the ITZ and cement matrix also gradually decreases and almost vanishes at $S = 44\%$. Hence, the peak value of $\kappa_{ITZ}/\kappa_{matrix}$ is found to gradually go down to finally completely vanish in Fig. 12. When S reaches 44%, the permeability of ITZ is close to that of the cement matrix, resulting in an almost constant value (1–2) of $\kappa_{ITZ}/\kappa_{matrix}$. In this case, the dilution and tortuosity effects will cause the ITZ not to contribute to an increase in the overall permeability of concrete, so a reduction in permeability at an increased amount of aggregates can be expected, as experimentally observed in [5].

4. Discussion

As an important phase in concrete, the ITZ has long been considered as a zone of weakness, in terms of both strength and fluid permeation [2]. Although the ITZ is known to have larger pores and to be more permeable than the cement matrix, its influence on the overall permeability of concrete is still uncertain.

In fact, contradictory experimental results are obtained by different researchers. The ITZ percolation theory predicts that concrete permeability will rise at increasing aggregate content and that a sudden increase in permeability should occur at a critical aggregate fraction when the more permeable ITZ regions surrounding the aggregates start to interconnect. This is confirmed by Halamickova's work [4], but an inverse trend is also reported in [5], indicating a decreasing permeability with the addition of aggregates into the cement paste. When more aggregates are introduced into cement paste for promoting the impermeability of the concrete, except for the ITZ effect, two other competing effects (dilution and tortuosity) should be accounted for. According to Shane [15], the ITZ will govern the ionic transport when the conductivity ratio of the ITZ and cement matrix is of the order of 10–20. Shane's work inspired us to study the quantitative difference between the permeability of the ITZ and that of the bulk cement paste, which had not been carried out yet but could provide a new insight into the controversial experimental results. A DEM-based simulation approach is used to achieve these objectives.

For cement in normal concrete ($w/c = 0.4$, particle size range from 1 μm to 30 μm), it is found that the permeability ratio of the ITZ to bulk paste ($\kappa_{ITZ}/\kappa_{matrix}$) is actually a function of the hydration degree. The

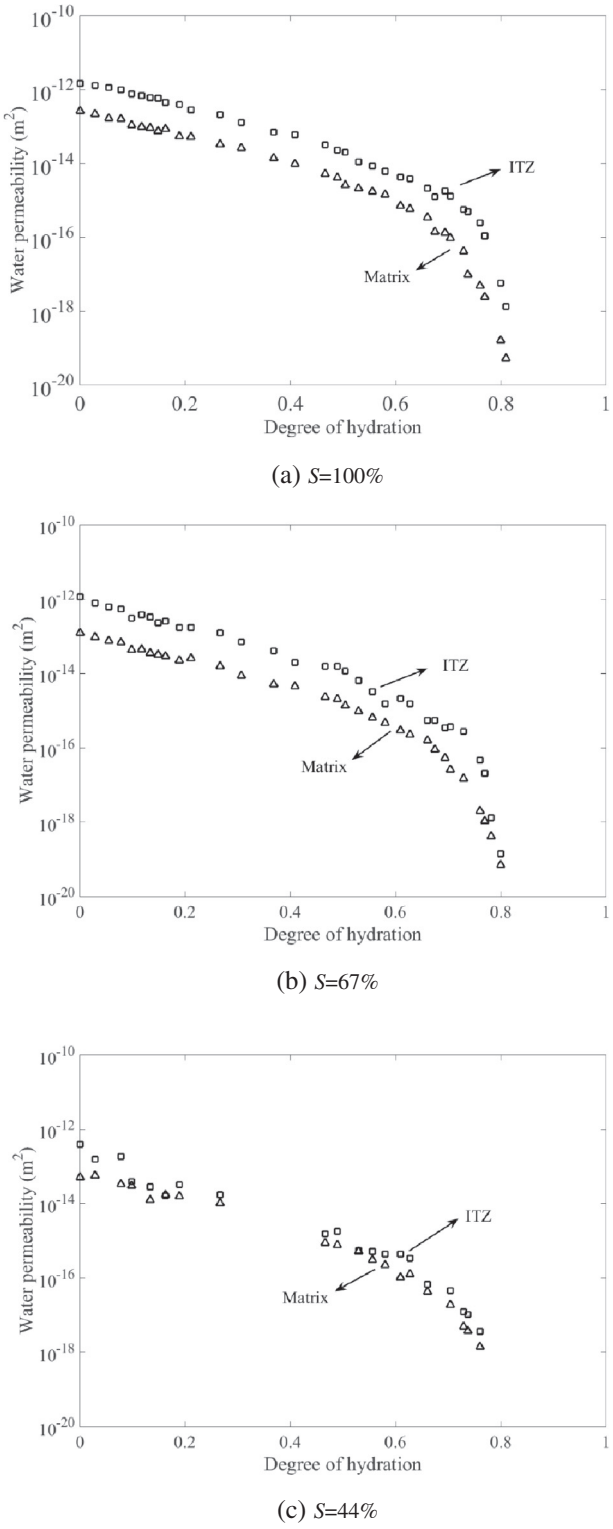

Fig. 11. Permeability of ITZ and matrix *versus* degree of hydration at various saturation degrees.

$\kappa_{ITZ}/\kappa_{matrix}$ curve reaches its peak value (about 52) at a degree of hydration of 0.76, which is larger than the threshold value proposed by Shane. It indicates that the ITZ effect is the dominant factor in this case. The origin of this peak is due to the different starting points of the pore de-percolation process, which can be expected to start earlier in the bulk because of the finer pore network structure. The $\kappa_{ITZ}/\kappa_{matrix}$ curve is in general below 10 in other hydration periods, implying the dilution

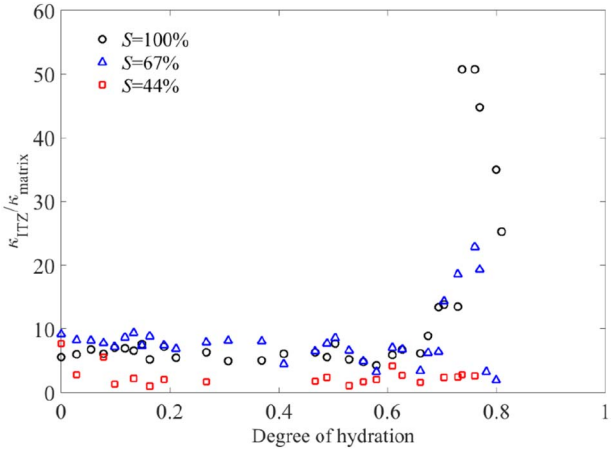

Fig. 12. $\kappa_{ITZ}/\kappa_{matrix}$ *versus* degree of hydration at various saturation degrees.

and tortuosity effects to dominate. This conforms to the observations published in [15]. Variation in the material parameters (*i.e.*, water/cement ratio and particle size range) leads to similar phenomena, but with a certain shift of the peak value. This is attributed to the fact that the pores in the ITZ and bulk matrix de-percolate at different overall DOH in different samples. Note that for a particle size range of 1 μm to 45 μm, an obvious peak is absent since the hydration process of this specimen becomes very slow and is almost negligible before reaching the de-percolation threshold, so the $\kappa_{ITZ}/\kappa_{matrix}$ curve remains on an almost constant level. Further, the effect of the water saturation degree on the permeability ratio is studied to represent practical conditions. It is found that the peak value of the $\kappa_{ITZ}/\kappa_{matrix}$ curve gradually decreases and finally completely vanishes when the saturation degree is reduced from 100% *via* 67% to 44%. This indicates that it is not likely that the ITZ would significantly enhance the permeability of concrete in this case.

The numerical approach used herein is restricted in some respects. In the first place, cracks existing in real 'virgin' concrete are not taken into account in this study. These shrinkage cracks will predominantly develop in the inner side of the ITZ region and interconnect with each other to form only a continuous transport path at high aggregate density, thereby facilitating fluid flow and promoting permeability. This may result in a lifting of the $\kappa_{ITZ}/\kappa_{matrix}$ curve as shown in Fig. 5. However, cracks are not easy to model since their locations and orientations in particularly loaded concrete vary a lot even in similar specimens. The interaction of such cracks and the pore channels make things even more complicated. It is therefore quite reasonable to have limited the number of variables in the present study rather than making the set up too complicated. In the second place, the thickness of the ITZ is kept constant in our simulations to be able comparing outcomes with those in [15]. Yet, previous studies have shown that the ITZ thickness depends on the material properties. Then, the sample has to be immersed into water for long periods of time to ensure its fully saturated state before conducting permeability measurements in practice. This surplus of water will inevitably lead to a continuing hydration process, a deficit in experimental approaches. However, this effect is not taken into account in this work and the microstructure obtained after hydration simulation is assumed to be unchanged. Moreover, the exposure to water during the permeability test is assumed not to affect the saturation degree of the specimen in this study. Finally, ITZ and bulk paste have to be distinguished to identify their respective contributions to the overall permeability of concrete, as intensively discussed herein. This treatment is somewhat artificial since the pores in the ITZ will actually also connect to the pores in the cement matrix. This is fundamental and therefore not a limitation of the present approach. The first two restrictions could possibly be eliminated in future research. Particularly explicitly considering micro-cracking in combination with porosity could enhance the methodology, although it is expected that the present day restrictions have not significantly affected the conclusions that can be drawn from this study.

5. Conclusions

The permeability ratio of the ITZ and the cement matrix is an important parameter that determines the influence of the ITZ on the permeability of concrete. This factor is thoroughly studied by simulating a 100 μm cement paste sandwiched structure between two parallel aggregate surfaces leading to ITZs with a constant width of 15 μm for different parameters, *i.e.*, hydration duration, water/cement ratio, cement particle size range and saturation degree. Note that the concrete scale was not modelled so effects such as dilution, tortuosity, aggregate size and shape were not considered in this paper.

Although the ITZ contains a higher porosity and thus has a higher local permeability than that of bulk paste, its net effect on the overall permeability of concrete is actually limited. Only in a narrow region of the hydration degree, a peak value is observed in the abovementioned permeability ratio curve. This undergoes a limited shift for different water/cement ratios and particle size ranges. Specifically, the ITZ dominates the flow transport through the specimen in this narrow range. Otherwise, the dilution and the tortuosity effects will exceed that of the ITZ. Even at a high aggregate fraction, whereby the ITZs would be interconnected or percolated, the relevant predictions by the percolation theory of increasing permeability and finally a dramatic increase can hardly be expected. Concrete in service easily loses water due to the humidity changes in the environment, resulting in a partially saturated specimen. The associated water saturation degree is found to reduce the difference in permeability of the ITZ and the cement matrix. Almost a constant permeability ratio between the ITZ and bulk paste at different hydration stages of 1–2 is observed at a water saturation degree of 44%. Therefore, the ITZ and ITZ percolation will probably not significantly promote the transport properties of concrete in practice.

Of course, micro-cracking along the ITZ of real concrete could be an intriguing factor in determining flow transport, particularly when ITZs are percolated. The study of combined porosity and micro-cracking effects would require large computer efforts and is therefore a topic for future research on 'compucrete' (computational concrete) as conducted herein.

Acknowledgements

The financial support from the China Scholarship Council (CSC) (No. 201206950005) to this work is gratefully acknowledged. The first author would like to thank Dr. Hong S. Wong (Imperial College London, UK) and Dr. Dale P. Bentz (National Institute of Standards and Technology, USA) for the discussion regarding influence of the interfacial transition zone on transport properties of cementitious materials.

References

[1] K.L. Scrivener, A.K. Crumbie, P. Laugesen, The interfacial transition zone (ITZ) between cement paste and aggregate in concrete, Interface Sci. 12 (2004) 411–421.
[2] K.L. Scrivener, K.M. Nemati, The percolation of pore space in the cement paste/aggregate interfacial zone of concrete, Cem. Concr. Res. 26 (1996) 35–40.
[3] D.N. Winslow, M.D. Cohen, D.P. Bentz, K.A. Snyder, E.J. Garboczi, Percolation and pore structure in mortars and concrete, Cem. Concr. Res. 24 (1994) 25–37.
[4] P. Halamickova, R.J. Detwiler, D.P. Bentz, E.J. Garboczi, Water permeability and chloride ion diffusion in Portland cement mortars: relationship to sand content and critical pore diameter, Cem. Concr. Res. 25 (1995) 790–802.
[5] H.S. Wong, M. Zobel, N.R. Buenfeld, R.W. Zimmerman, Influence of the interfacial transition zone and microcracking on the diffusivity, permeability and sorptivity of cement-based materials after drying, Mag. Concr. Res. 61 (2009) 571–589.
[6] A. Delagrave, J.P. Bigas, J.P. Ollivier, J. Marchand, M. Pigeon, Influence of the interfacial zone on the chloride diffusivity of mortars, Adv. Cem. Based Mater. 5 (1997) 86–92.
[7] L.M. Schwartz, E.J. Garboczi, D.P. Bentz, Interfacial transport in porous media: application to DC electrical conductivity of mortars, J. Appl. Phys. 78 (1995) 5898–5908.

[8] E.J. Garboczi, L.M. Schwartz, D.P. Bentz, Modeling the influence of the interfacial zone on the DC electrical conductivity of mortar, Adv. Cem. Based Mater. 2 (1995) 169–181.
[9] K. Wu, L.L. Xu, G.D. Schutter, H.S. Shi, G. Ye, Influence of the interfacial transition zone and interconnection on chloride migration of Portland cement mortar, J. Adv. Concr. Technol. 13 (2015) 169–177.
[10] J.J. Zheng, H.S. Wong, N.R. Buenfeld, Assessing the influence of ITZ on the steady-state chloride diffusivity of concrete using a numerical model, Cem. Concr. Res. 39 (2009) 805–813.
[11] M.Z. Zhang, G. Ye, K. van Breugel, Multiscale lattice Boltzmann-finite element modelling of chloride diffusivity in cementitious materials. Part II: simulation results and validation, Mech. Res. Commun. 58 (2014) 64–72.
[12] S.D. Abyaneh, H.S. Wong, N.R. Buenfeld, Modelling the diffusivity of mortar and concrete using a three-dimensional mesostructured with several aggregate shapes, Comput. Mater. Sci. 78 (2013) 63–73.
[13] P. Stroeven, A stereological approach to roughness of fracture surfaces and tortuosity of transport paths in concrete, Cem. Concr. Compos. 22 (2000) 331–341.
[14] E.J. Garboczi, D.P. Bentz, Modelling of the microstructure and transport properties of concrete, Constr. Build. Mater. 10 (1996) 293–300.
[15] J.D. Shane, T.O. Mason, H.M. Jennings, E.J. Garboczi, D.P. Bentz, Effect of the interfacial transition zone on the conductivity of Portland cement mortars, J. Am. Ceram. Soc. 83 (2000) 1137–1144.
[16] M. Zalzale, P.J. McDonnald, K.L. Scrivener, A 3D lattice Boltzmann effective media study: understanding the role of C-S-H and water saturation on the permeability of cement paste, Model. Simul. Mater. Sci. Eng. 21 (2013) 085016.
[17] Z.A. Kameche, F. Ghomari, M. Choinska, A. Khelidj, Assessment of liquid water and gas permeability of partially saturated ordinary concrete, Constr. Build. Mater. 65 (2014) 551–565.
[18] K. Li, M. Stroeven, P. Stroeven, L.J. Sluys, Investigation of liquid water and gas permeability of partially saturated cement paste by DEM approach, Cem. Concr. Res. 83 (2016) 104–113.
[19] K. Li, P. Stroeven, L.B.N. Le, Methodology for porosimetry in virtual cementitious composites to economically and reliably estimate permeability, Image Anal. Stereol. 34 (2015) 73–86.
[20] H.X.D. Lee, H.S. Wong, N.R. Buenfeld, Self-sealing of cracks in concrete using superabsorbent polymers, Cem. Concr. Res. 79 (2016) 194–208.
[21] L.C. Wang, T. Ueda, Mesoscale modelling of the chloride diffusion in cracks and cracked concrete, J. Adv. Concr. Technol. 9 (2011) 241–249.
[22] Z. Wu, H.S. Wong, N.R. Buenfeld, Influence of drying-induced microcracking and related size effects on mass transport properties of concrete, Cem. Concr. Res. 68 (2015) 35–48.
[23] Z. Wu, H.S. Wong, N.R. Buenfeld, Transport properties of concrete after drying-wetting regimes to elucidate the effects of moisture content, hysteresis and microcracking, Cem. Concr. Res. 98 (2017) 136–154.
[24] P. Stroeven, K. Li, L.B.N. Le, H. He, M. Stroeven, Capabilities for property assessment on different levels of the micro-structure of DEM-simulated cementitious materials, Constr. Build. Mater. 88 (2015) 105–117.
[25] J.J. Zheng, C.Q. Li, Three-dimensional aggregate density in concrete with wall effect, ACI Mater. J. 99 (2002) 568–575.
[26] H.S. Wong, N.R. Buenfeld, Patch microstructure in cement-based materials: fact or artefact? Cem. Concr. Res. 36 (2006) 990–997.
[27] L.B.N. Le, M. Stroeven, L.J. Sluys, P. Stroeven, A novel numerical multi-component model for simulating hydration of cement, Comput. Mater. Sci. 78 (2013) 12–21.
[28] H.M. Jennings, A model for the microstructure of calcium silicate hydrate in cement paste, Cem. Concr. Res. 30 (2000) 101–116.
[29] H.M. Jennings, Refinements to colloid model of C-S-H in cement: CM-II, Cem. Concr. Res. 38 (2008) 275–289.
[30] P. Stroeven, L.B.N. Le, L.J. Sluys, H. He, Porosimetry by double random multiple tree structuring, Image Anal. Stereol. 31 (2012) 55–63.
[31] L.B.N. Le, Micro-level Porosimetry of Virtual Cementitious Materials — Structural Impact on Mechanical and Durability Evolution, Ph.D. Thesis Delft University of Technology, Delft, The Netherlands, 2015.
[32] A.C.A. Muller, K.L. Scrivener, A.M. Gajewicz, P.J. McDonnald, Densification of C-S-H measured by ^{1}H NMR relaxometry, J. Phys. Chem. C 117 (2013) 403–412.
[33] M. Zalzale, Water Dynamics in Cement Paste: Insights From Lattice Boltzmann Modelling, Ph.D. Thesis Ecole Polytechnique Federale De Lausanne, Lausanne, Switzerland, 2014.
[34] K. Li, P. Stroeven, M. Stroeven, L.J. Sluys, Estimating permeability of cement paste using pore characteristics obtained from DEM-based modelling, Constr. Build. Mater. 126 (2016) 740–746.
[35] H.Y. Ma, Mercury intrusion porosimetry in concrete technology: tips in measurement, pore structure parameter acquisition and application, J. Porous Mater. 21 (2014) 207–215.
[36] M.R. Nokken, R.D. Hooton, Using pore parameters to estimate permeability or conductivity of cocnrete, Mater. Struct. 41 (2008) 1–16.
[37] M. Stroeven, Discrete Numerical Modelling of Composite Materials — Application to Cementitious Materials, Ph.D. Thesis Delft University of Technology, Delft, The Netherlands, 1999.